

Carbon-rich hexagonal (BN)C alloys

M. R. Uddin, J. Li, J. Y. Lin, and H. X. Jiang^{a)}

Department of Electrical and Computer Engineering, Texas Tech University, Lubbock, Texas 79409, USA

(Received 26 March 2015; accepted 20 May 2015; published online 1 June 2015)

Thin films of hexagonal boron nitride carbon, $h\text{-(BN)}_{1-x}\text{(C}_2\text{)}_x$, alloys in the C-rich side have been synthesized by metal-organic chemical vapor deposition (MOCVD) on c -plane sapphire substrates. X-ray diffraction measurements confirmed single hexagonal phase of $h\text{-(BN)}_{1-x}\text{(C}_2\text{)}_x$ epilayers. Electrical transport and Raman spectroscopy measurements results revealed evidences that homogeneous $h\text{-(BN)}_{1-x}\text{(C}_2\text{)}_x$ alloys with $x \geq 95\%$ can be synthesized by MOCVD at a growth temperature of 1300 °C. The variable temperature Hall-effect measurements suggested that a bandgap opening of about 93 meV with respect to graphite has been obtained for $h\text{-(BN)}_{1-x}\text{(C}_2\text{)}_x$ with $x = 0.95$, which is consistent with the expected value deduced from the alloy dependence of the energy gap of homogeneous $h\text{-(BN)}_{1-x}\text{(C}_2\text{)}_x$ alloys. Atomic composition results obtained from x-ray photoelectron spectroscopy measurements revealed that the carrier type in C-rich $h\text{-(BN)}_{1-x}\text{(C}_2\text{)}_x$ alloys is controlled by the *stoichiometry* ratio between the B and N via changing the V/III ratio during the growth. The demonstration of bandgap opening and conductivity control in C-rich $h\text{-(BN)}_{1-x}\text{(C}_2\text{)}_x$ alloys provide feasibilities for realizing technologically significant devices including infrared (IR) emitters and detectors active from near to far IR and multi-spectral IR emitters and detectors.
 © 2015 AIP Publishing LLC. [<http://dx.doi.org/10.1063/1.4921931>]

I. INTRODUCTION

Hexagonal boron nitride ($h\text{-BN}$) is a layer-structured semiconductor material with a bandgap energy (~ 6.4 eV) that is comparable to that of AlN (~ 6.1 eV) with excellent thermal, mechanical, and optical properties.^{1–6} Hexagonal $(\text{BN})_{1-x}(\text{C}_2)_x$ alloys hold the unique advantages of identical crystalline structure (hexagonal) and excellent in-plane lattice constant match between $h\text{-BN}$ and graphite ($a_{\text{graphite}} = 2.46$ Å and $a_{h\text{-BN}} = 2.50$ Å, $c_{\text{graphite}} = 6.70$ Å, and $c_{h\text{-BN}} = 6.66$ Å). Moreover, both $h\text{-BN}$ and graphite have similar thermal expansion coefficients and high melting temperatures (~ 3000 °C for $h\text{-BN}$ ⁷ and ~ 3500 – 4500 °C for graphite⁸). We are using the expression of $(\text{BN})_{1-x}(\text{C}_2)_x$ for these alloys to take into consideration the fact that C atoms tend to incorporate as C-C (C_2) pairs.^{9,10} The $h\text{-(BN)}_{1-x}\text{(C}_2\text{)}_x$ alloys in the C-rich side have the potential to provide an unprecedented degree of freedom in the infrared (IR) detector and electronic device design. As the BN composition increases or C composition decreases, the energy gap for $h\text{-(BN)}_{1-x}\text{(C}_2\text{)}_x$ alloy gradually increases from zero for graphene to ~ 6.4 eV for $h\text{-BN}$. This spectral range is even larger than that of the InAlGaN alloy system, which provides a tunable bandgap from around 0.7 eV (InN) to 3.4 eV (GaN) to 6.1 eV (AlN). From an electrical properties perspective, this alloy system ranges from highly insulating semiconductor (undoped $h\text{-BN}$) to semi-metal (graphite), and therefore, a large range of conductivity control can be obtained.⁹ The bandgap energy tunability in the C-rich side could offer IR detectors with cut-off wavelengths covering from short wavelength IR (SWIR: 1–3 μm) to very long wavelength (VLWIR: 14–30 μm) range. Furthermore, the C-rich $h\text{-(BN)}_{1-x}\text{(C}_2\text{)}_x$ alloys would address the major challenges facing the

emerging 2D materials and open up new realms for novel physical properties and devices exploration.

However, one of the critical issues of any alloy material system is the phase separation and the composition range where homogeneous alloys can be formed. Phase separation could occur in the formation of alloys due to the difference in lattice constants of the constituents or bond energies between the atoms. Growth of (BN)C alloy is challenging due to the strong inter-atomic bonds between B-N and C-C, which have respective bond energies of 4.0 eV (B-N) and 3.71 eV (C-C) compared with values of 2.83 eV for the C-N bond and 2.59 eV for the C-B bond.^{10,11} The large bond energy differences tend to cause phase separation in certain range of x for $h\text{-(BN)}_{1-x}\text{(C}_2\text{)}_x$ alloys.⁹ A recent theoretical calculation on monolayer $(\text{BN})_{1-x}(\text{C}_2)_x$ alloys suggested a low solubility of BN in graphene or C in BN.¹² Despite the challenges, we have successfully synthesized homogeneous (BN)-rich $h\text{-(BN)}_{1-x}\text{(C}_2\text{)}_x$ alloys ($x \leq 3.2\%$) by metal organic chemical vapor deposition (MOCVD) at relatively high growth temperatures (~ 1300 °C) and demonstrated bandgap and electrical conductivity tuning in the alloy system.^{9,13} However, very little work has been reported on synthesizing C-rich $h\text{-(BN)C}$ alloys. C-rich $h\text{-(BN)C}$ thin films (of ~ 1 nm in thickness) with a maximum carbon concentration of $\sim 94.4\%$ have been previously synthesized by CVD on Cu foil at a growth temperature of 1000 °C.¹⁴ It was shown that $h\text{-(BN)C}$ materials on Cu foil were phase separated to randomly distributed domains of $h\text{-BN}$ and C phases, rendering these materials less suitable for technologically significant electronic and photonic device applications.

In this work, we report the synthesis of wafer scale $h\text{-(BN)}_{1-x}\text{(C}_2\text{)}_x$ alloys in the C-rich side on c -plane sapphire substrates by MOCVD at a growth temperature of 1300 °C. Hall-effect in conjunction with x-ray photoelectron spectroscopy (XPS) measurements revealed that the carrier type in

^{a)}Email: hx.jiang@ttu.edu

C-rich $h\text{-(BN)}_{1-x}\text{(C}_2\text{)}_x$ alloys is controlled by the *stoichiometry* ratio between the B and N via changing the V/III ratio during the growth. Variable temperature Hall-effect and Raman spectroscopy studies suggested that homogenous $h\text{-(BN)}_{1-x}\text{(C}_2\text{)}_x$ alloy can be formed for $x \geq 0.95$ and the bandgap of $h\text{-(BN)}_{1-x}\text{(C}_2\text{)}_x$ alloy with $x=0.95$ is about 93 meV. The present results could serve as a guideline for obtaining bandgap tuning in single or few layer graphene, as the bandgap opening in graphene and graphite follows a fairly similar process.¹⁵

II. EXPERIMENT

Figure 1(a) shows the schematic of the layer structure. Epitaxial layers of $h\text{-(BN)}_{1-x}\text{(C}_2\text{)}_x$ alloys ($x \sim 0.92$ to 0.95) of about 100 nm in thickness were synthesized on $h\text{-BN}/c\text{-plane}$ sapphire substrates. Triethylboron (TEB), ammonia (NH_3), and propane (C_3H_8) were used as B, N, and C *precursors*, respectively. Samples were grown using nitrogen as a carrier gas at 1300 °C. Eleven samples were grown using NH_3 flow rates of 1.0, 1.2, 1.4, 1.6, 1.8, 2.0, 2.2, 2.4, 2.6, 2.8, and 3.0 standard cubic centimeters per minute (sccm). Both TEB and C_3H_8 flow rates were kept constant at 0.18 sccm and 20 sccm, respectively. Crystalline structure was characterized by x-ray diffraction (XRD) measurements. Atomic composition of B, N, and C were determined using XPS, which is a quantitative spectroscopic technique to determine the elemental composition in a material system. Room temperature Hall-effect measurements were used to measure the resistivity, carrier mobility and carrier concentration. Variable temperature Hall-effect measurements were attempted to probe the intrinsic bandgaps of the C-rich $h\text{-(BN)}_{1-x}\text{(C}_2\text{)}_x$ alloys, while Raman spectroscopy measurements were utilized to study the phase separation effect. The Raman spectra were collected at room temperature by a Bruker Senterra dispersive Raman spectrometer using a 532 nm (2.33 eV Ar ion laser) excitation source. All the samples were measured at the same time under the same experimental conditions.

III. RESULTS AND DISCUSSION

Figures 1(b) and 1(c) show the optical micrographs of a graphite sample and an $h\text{-(BN)}_{1-x}\text{(C}_2\text{)}_x$ alloy sample with $x=0.95$ (grown under 1 sccm NH_3 flow rate). Based on the bandgap value of graphite (zero gap), $h\text{-(BN)}_{1-x}\text{(C}_2\text{)}_x$ epilayers with large values of x should appear black under the visible light. Figure 1(d) shows X-ray diffraction (XRD) θ - 2θ scans of $h\text{-(BN)}_{1-x}\text{(C}_2\text{)}_x$ samples grown under 1, 2, and 3 sccm NH_3 flow rates (corresponding carbon concentrations are $\sim 95.0\%$, 93.3%, and 91.5%, respectively), revealing a lattice constant of $c=6.73 \text{ \AA}$ for all samples, which closely matches with a value of $c=6.70 \text{ \AA}$ for graphite.¹⁶ No other diffraction peaks were observed, which confirms the hexagonal crystalline structure of the $(\text{BN})_{1-x}(\text{C}_2)_x$ epilayers. The slight increase in “ c ” lattice constant over graphite may be related to the fact that these films were grown on $h\text{-BN}$ template and experience a “compressive”-like strain in the a -plane. Another possibility is that the crystalline quality of $h\text{-(BN)}_{1-x}\text{(C}_2\text{)}_x$ alloys is not yet as good as $h\text{-BN}$ epilayers. As we have noted previously, the “ c ” lattice constant of $h\text{-BN}$ epilayers decreases and approaches the bulk value as the crystalline quality improves. A similar trend is expected for $h\text{-(BN)}_{1-x}\text{(C}_2\text{)}_x$ alloys. A typical optical microscope image (Fig. 1(e)) shows that the film is quite uniform with almost no color variation.

XPS depth profile measurements were performed on three representative $h\text{-(BN)}_{1-x}\text{(C}_2\text{)}_x$ epilayers grown under 1, 2, and 3 sccm NH_3 flow rates. Samples were successively etched using low energy (500 V) Ar^+ ions and high resolution tight scans were taken for sufficiently long time after each etching step. Initial survey scans show no other transitions except B 1s, N 1s, and C 1s peaks, meaning that there are no impurities such as oxygen in our samples. All data were analyzed consistently using Multipak software package to determine the atomic compositions.^{9,13} Table I shows average B, N, and C concentrations for the $h\text{-(BN)}_{1-x}\text{(C}_2\text{)}_x$ epilayers grown under 1, 2, and 3 sccm NH_3 flow rates obtained from multiple measurements on a given sample. Quantification of errors was obtained from variation in XPS

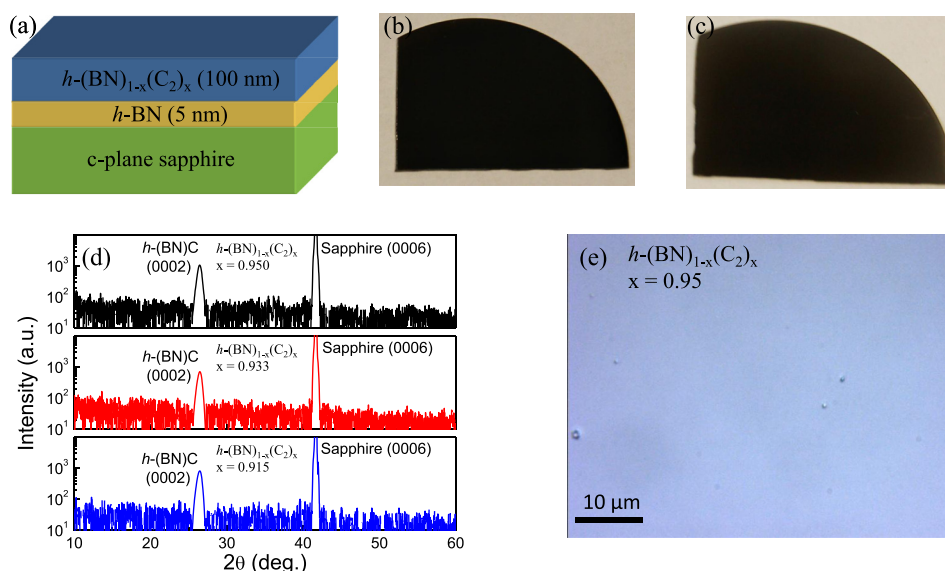


FIG. 1. (a) Schematic of the $h\text{-(BN)}_{1-x}\text{(C}_2\text{)}_x$ epilayer. Optical micrographs of (b) graphite and (c) $h\text{-(BN)}_{1-x}\text{(C}_2\text{)}_x$ alloy with $x=0.95$. (d) XRD θ - 2θ scans of the $h\text{-(BN)}_{1-x}\text{(C}_2\text{)}_x$ epilayers grown on $c\text{-plane}$ sapphire substrates under 1, 2, and 3 sccm NH_3 flow rates. (e) Optical image of the $h\text{-(BN)}_{1-x}\text{(C}_2\text{)}_x$ alloy with $x=0.95$.

TABLE I. Average atomic compositions of $h\text{-(BN)}_{1-x}\text{(C}_2)_x$ epilayers obtained from multiple measurements of a given sample.

NH ₃ flow rate (sccm)	At. % B	At. % N	At. % C
1	3.0 ± 0.2	2.0 ± 0.2	95.0 ± 0.3
2	3.6 ± 0.2	3.1 ± 0.2	93.3 ± 0.5
3	3.9 ± 0.3	4.6 ± 0.3	91.5 ± 0.6

spectra when acquired from different regions of a given sample. It is noticeable that atomic compositions are fairly stable across the sample, which suggests that our samples are uniform. XPS results show that x (C mole fraction) decreases almost linearly with the increase in NH₃ flow rate (sccm). This is due to the increase in BN fraction in the $h\text{-(BN)}_{1-x}\text{(C}_2)_x$ epilayers with an increase in N (NH₃ flow rate). Consequently, a linear interpolation was used to estimate the carbon concentration in other samples. It is important to note from Table I that we can vary slightly the *stoichiometry* ratio between B and N in $h\text{-(BN)}_{1-x}\text{(C}_2)_x$ epilayers by varying the V/III ratio (or the NH₃ flow rate) and that the N concentration increases with increasing the NH₃ flow rate.

There are distinctive differences between C-rich $h\text{-(BN)}_{1-x}\text{(C}_2)_x$ alloys and conventional III-nitride alloys. The formation of ternary $\text{In}_x\text{Ga}_{1-x}\text{N}$ or $\text{Al}_x\text{Ga}_{1-x}\text{N}$ alloys involves the random mixing of group-III atoms only. However, $h\text{-(BN)}_{1-x}\text{(C}_2)_x$ alloys are formed through the incorporation of group-III (B) and group-V (N) atoms into the group-IV graphite (C), in which B and N may also serve as dopants. In a simplified picture of understanding and assuming both N and B incorporate *substitutionally*, N could replace C to give rise to n-type conductivity and B could replace C to give rise to p-type conductivity. Consequently, a slight deviation from the ideal (1:1) *stoichiometry* ratio between B and N could have strong influences on the conductivity type of C-rich $h\text{-(BN)}_{1-x}\text{(C}_2)_x$.

Room temperature Hall-effect measurements were used to measure the resistivity, carrier mobility and carrier concentration. Efforts were made to minimize the impact of possible sample non-uniformity on the measured carrier type

and concentrations. This was achieved via the use of square shaped sample geometry with small ohmic contacts fabricated on the four corners of the sample surface.^{9,13,17–19} The microscope image of a fabricated $h\text{-(BN)}_{1-x}\text{(C}_2)_x$ alloy ($x=0.95$) sample with four ohmic contacts (Ni/Au bilayers) on the corners is shown in Fig. 2(a). The ratio of the contact size (c) to the sample length scale (L) is about 1/7.5, a configuration which is expected to provide a high confidence in the measured carrier type.¹⁷ Figure 2(b) shows the room temperature mobility and carrier concentration of $h\text{-(BN)}_x\text{C}$ epilayers as functions of the NH₃ flow rate employed during the MOCVD growth obtained using Hall-effect measurements. Remarkably, the results shown in Fig. 2(b) indicate that the carrier type is p-type for samples synthesized under NH₃ flow rates below 2.1 sccm and is n-type for the samples synthesized under NH₃ flow rates above 2.1 sccm. As we discussed, one unique aspect of C-rich $h\text{-(BN)}_{1-x}\text{(C}_2)_x$ alloys is that they can be viewed as B and N co-doped materials, in which B atoms behave as p-type dopants while N atoms behave as n-type dopants. When synthesized under NH₃ flow rates below 2.1 sccm, there are fewer N atoms than B atoms in the materials and hence a p-type conductivity prevails. Supplying more N atoms to the reaction zone by increasing the NH₃ flow rate to above 2.1 sccm produces materials containing more N atoms than B atoms and hence n-type conductivity dominates. This is further verified by the XPS measurement results shown in Table I which indicate that the samples synthesized under 1 and 2 sccm NH₃ flow rates have lower N concentration ([N] = 2.0%) than B ([B] = 3.0%) for 1 sccm NH₃ flow rate and ([N] = 3.1%) than B ([B] = 3.6%) for 2 sccm NH₃ flow rate, while the sample synthesized under 3 sccm NH₃ flow rate has higher N concentration ([N] = 4.6%) than B ([B] = 3.9%). At NH₃ = 2.1 sccm, the concentrations of N atoms and B atoms are equal and a transition from p- to n-type conductivity occurs. In other word, when grown under an NH₃ flow rate of about 2.1 sccm, C-rich $h\text{-(BN)}_{1-x}\text{(C}_2)_x$ alloys have a 1:1 *stoichiometry* ratio between B atoms and N atoms, [B] = [N]. The observed background carrier concentrations at room temperature for both p- and n-type C-rich $h\text{-(BN)}_{1-x}\text{(C}_2)_x$ epilayers are relatively high ($\sim 1.5 \times 10^{20} \text{ cm}^{-3}$), which can be accounted for

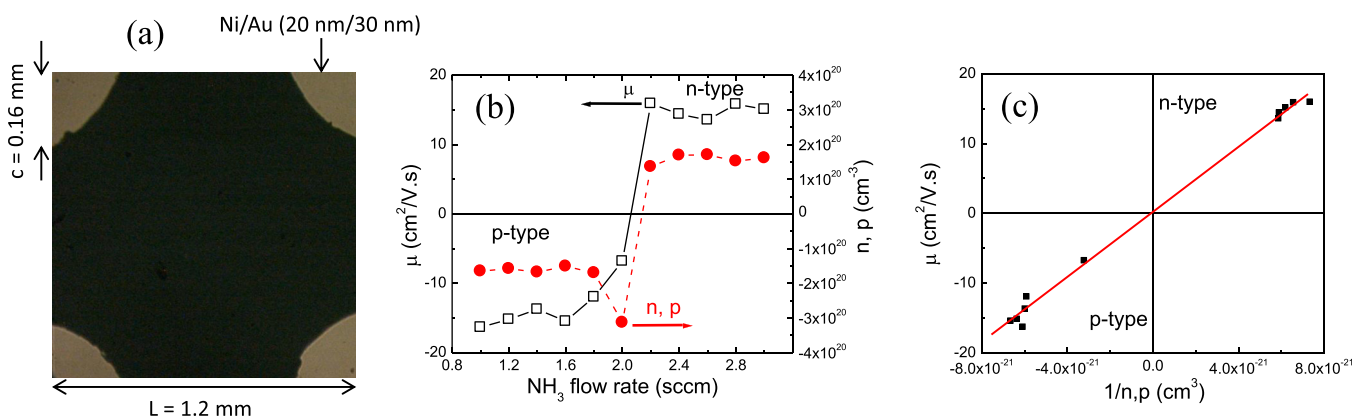


FIG. 2. (a) The microscope image of a $h\text{-(BN)}_{1-x}\text{(C}_2)_x$ alloy ($x=0.95$) sample with ohmic contacts (Ni/Au bilayers) fabricated on the four corners for van der Pauw–Hall measurements. (b) Mobility and carrier concentration of $h\text{-(BN)}_{1-x}\text{(C}_2)_x$ epilayers grown under different NH₃ flow rates. The carrier type in the alloys is p-type for NH₃ flow rates below 2.1 sccm and changes to n-type for NH₃ flow rates above 2.1 sccm. (c) Carrier mobility as a function of inverse concentration plot, μ vs. $(1/n, 1/p)$, showing the same dependence for electrons and holes.

by the following two factors: (1) the doping levels of N or B “dopants” are very high since B, N, C atoms form alloys and even a small local compositional fluctuation of 0.5% would translate to a doping level of $5 \times 10^{19} \text{ cm}^{-3}$ and (2) the energy bandgaps of C-rich $h\text{-(BN)C}$ alloys are small and the energy level of the N donors (B acceptors) in C-rich $h\text{-(BN)C}$ alloys is expected to be very shallow or possibly even lie within the conduction (valence band).

The electron and hole mobilities (μ_e or μ_h) and concentrations (n or p) are quite comparable and their dependence on the NH_3 flow rate are almost symmetric around $\text{NH}_3 = 2.1$ sccm. The results suggest that the effective masses of electrons and holes in C-rich $h\text{-(BN)}_{1-x}(\text{C}_2)_x$ alloys must be comparable, similar to the case of single sheet $h\text{-BN}$.^{20,21} However, it is not clear why the free carrier concentrations are almost independent of the NH_3 flow rate except in the transition region. Self-compensation effect could be a possible cause for this behavior, similar to that observed in heavily Ge and C co-doped GaAs thin films.^{22,23}

It is expected that ionized impurity scattering is a dominant mechanism in determining the carrier mobilities at room temperature in C-rich $h\text{-(BN)}_{1-x}(\text{C}_2)_x$ alloys. In this case, the scattering rate, γ , is proportional to the ionized impurity concentration, which, to the first order is the same as the free carrier concentration due to small energy bandgap. It is thus

$$\gamma \propto N_D^+, \quad N_A^- \propto (n, p). \quad (1)$$

So, for electrons,

$$\begin{aligned} \mu_e &\propto \frac{1}{r} \propto \frac{1}{N_D^+} \propto \frac{1}{n}, \\ \mu_e &= \frac{C_n}{n}. \end{aligned} \quad (2)$$

Since $\mu_e n = \frac{\sigma_n}{e}$, we therefore have $C_n = \frac{\sigma_n}{e} = \frac{1}{e\rho_n}$, where σ_n and ρ_n are the n-type conductivity and resistivity, respectively. Based on Eq. (2), a linear relationship between μ_e and $1/n$ is expected with a slope of C_n . Similarly for holes we have

$$\begin{aligned} \mu_h &\propto \frac{1}{r} \propto \frac{1}{N_A^-} \propto \frac{1}{p}, \\ \mu_h &= \frac{C_p}{p}, \end{aligned} \quad (3)$$

where $C_p = \frac{\sigma_p}{e} = \frac{1}{e\rho_p}$, σ_p , and ρ_p are the p-type conductivity and resistivity, respectively. Therefore, a linear relationship between μ_h and $1/p$ is also expected with a slope of C_p . In Fig. 2(c), we plot mobility vs. the inverse of carrier concentration, μ_e vs. n^{-1} and μ_h vs. p^{-1} . Although the experimental data points are clustered at the high carrier concentration regions, linear relationships between μ_e and $1/n$ and μ_h and $1/p$ are evident with $C_n = C_p$. The fact that the linear fit line passing through all the data points as well as the origin further suggests that the results are consistent with Eqs. (2) and (3). Based on the results shown in Fig. 2(c), we can draw two conclusions: (1) the conductivity is similar for both n- and p-type samples; and (2) the carrier mobility depends

only on the carrier concentration near room temperature. Room temperature mobility for both p- and n-type $h\text{-(BN)}_{1-x}(\text{C}_2)_x$ epilayers are $\sim 15 \text{ cm}^2/\text{V}\cdot\text{s}$, which is approximately one order lower than B- or N-doped single layer graphene,^{24,25} however is comparable to or slightly higher than atomic layers of $h\text{-(BN)C}$ materials containing separated BN and C domains.¹⁴ The reason for a lower carrier mobility of our samples compared to B- or N-doped single layer graphene is due to the much higher free carrier concentrations in these alloys.

Figure 3(a) shows the temperature dependence of the free hole concentration (p) for the $h\text{-(BN)}_{1-x}(\text{C}_2)_x$ sample with $x=0.95$ (corresponding to 1 sccm NH_3 flow rate) obtained from Van der Pauw Hall-effect measurements in the temperature range of 175–800 K. The temperature dependence of the carrier concentration follows that of a very

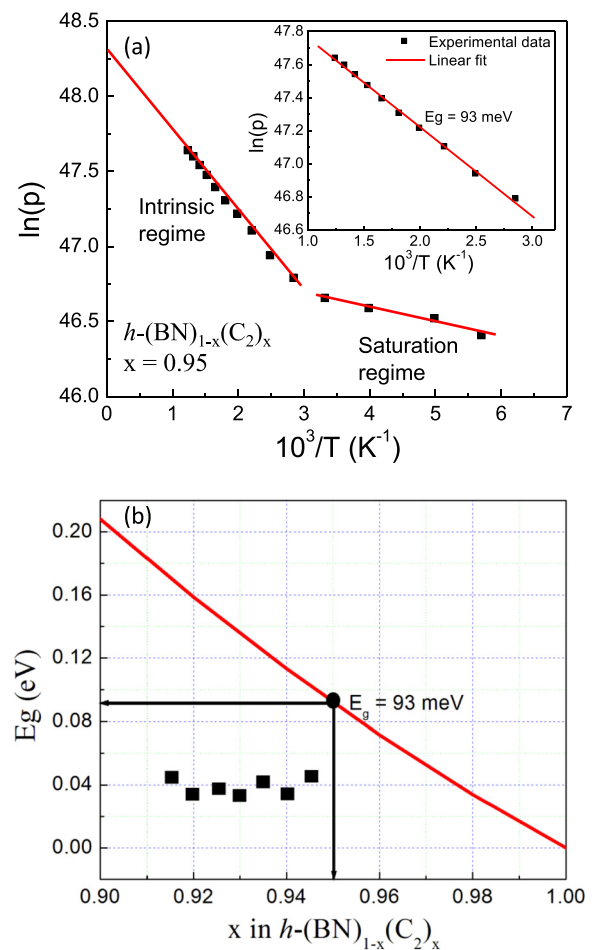


FIG. 3. (a) Temperature dependent hole concentration plotted in the scale of $\ln(p)$ vs. $1/T$ for an $h\text{-(BN)}_{1-x}(\text{C}_2)_x$ sample with $x=0.95$. The temperature dependence of the free carrier concentration shows a typical behavior of narrow gap semiconductors consisting of both saturation and intrinsic carrier conduction regime. Inset shows $\ln(p)$ vs. $1/T$ plot for the intrinsic region, from which a bandgap $E_g \sim 93 \text{ meV}$ is obtained. (b) Plot of the bandgap energy of $h\text{-(BN)}_{1-x}(\text{C}_2)_x$ alloys vs. carbon concentration (x) in the C-rich side obtained from Eq. (5) with $E_g(h\text{-BN}) = 6.4 \text{ eV}$, $E_g(\text{C}) = 0 \text{ eV}$, and the bowing parameter of $b = 4.8 \text{ eV}$. The activation energy (or the bandgap) value of $h\text{-(BN)}_{1-x}(\text{C}_2)_x$ with $x=0.95$ is marked as a solid circle on the plot of the band gap variation of $h\text{-(BN)}_{1-x}(\text{C}_2)_x$ with x . Activation energies of $h\text{-(BN)}_{1-x}(\text{C}_2)_x$ epilayers with $x < 0.95$ are also shown as solid squares, which deviate from the plot of the band gap variation of $h\text{-(BN)}_{1-x}(\text{C}_2)_x$ with x .

typical of narrow bandgap semiconductor with two distinct regimes.²⁶ In the medium or low temperature region, nearly all acceptors are ionized, the carrier concentration is nearly saturated and independent of (or only weakly depend on) the temperature. In the high temperature region, the carrier concentration is nearly intrinsic. The crossover from the saturation to the intrinsic conduction regime occurs around 350 °K. The inset of Fig. 3(a) shows the Arrhenius plot of the carrier concentration in the intrinsic conduction regime, in which the hole concentration (p) and energy gap (E_g) can be expressed in terms of temperature as

$$p \propto \exp\left(-\frac{E_g}{2k_b T}\right), \quad (4)$$

where k_b is the Boltzman constant. The fitted value of E_g obtained for the h -(BN)_{1-x}(C₂)_x alloy ($x=0.95$) is ~ 93 meV.

Bandgap opening in graphene by doping with B and N atoms has been demonstrated experimentally through the measurement of transistor current.^{24,25,27} Recent theoretical calculations²⁸ suggest that it is possible to tune the bandgap in graphene directly via BN doping. Here, we have demonstrated the bandgap opening in graphite via alloying with B and N atoms. The bandgap value obtained from Fig. 3(a) can be further confirmed by comparing the measured E_g value with that of expected. The expected bandgap variation of homogenous h -(BN)_{1-x}(C₂)_x alloys with x is plotted in Fig. 3(b) for the C-rich side and follows the relation⁹

$$E_g[h-(BN)_{1-x}(C_2)_x] = (1-x)E_g(h-BN) + xE_g(C) - b(1-x)x, \quad (5)$$

where values of $E_g(h-BN) = 6.4$ eV, $E_g(C) = 0$ eV, and the bowing parameter, $b = 4.8$ eV were used. Based on Eq. (5) and Fig. 3(b), for an h -(BN)_{1-x}(C₂)_x alloy ($x=0.95$), $E_g = 91$ meV is deduced, which agrees almost perfectly with a value of ~ 93 meV obtained from the temperature dependent carrier concentration presented in the inset of Fig. 3(a). This excellent agreement between the measured and expected bandgap values provides strong evidence that homogenous h -(BN)_{1-x}(C₂)_x alloys with $x \geq 0.95$ can be synthesized by MOCVD at a growth temperature of 1300 °C. The bowing parameter, b , was obtained by fitting Eq. (5) using $E_g(h-BN)$ ($x=0$) = 6.4 eV, $E_g(\text{graphite})$ ($x=1$) = 0 eV, and $E_g(\text{BNC}_2)$ ($x=0.5$) = 2.0 eV,²⁹ which was also used to describe the bandgap variation in (BN)-rich h -(BN)C alloys.⁹ Although the bowing parameter, b , of h -(BN)C alloys is still not very certain at this point, the excellent agreement between the energy gap values deduced from Eq. (5) and Fig. 3(b) and from Hall-effect measurement results in Fig. 3(a) seems to suggest that Eq. (5) and the bowing parameter used quite satisfactorily describe the energy band gap variation of h -(BN)_{1-x}(C₂)_x alloys.

We have also carried out the temperature dependence of the free carrier concentration in h -(BN)_{1-x}(C₂)_x epilayers with $x < 0.95$. The measured thermal activation energies for h -(BN)_{1-x}(C₂)_x epilayers with $x < 0.95$ are plotted in Fig. 3(b) and vary from ~ 32 meV to ~ 45 meV. These values deviate from the solid curve shown in Fig. 3(b), which indicates that

the activation energies obtained for the h -(BN)_{1-x}(C₂)_x epilayers with $x < 0.95$ are similar to those of lightly B- or N-doped graphite. This is probably an indication that phase separation and the formation of separate C-C and B-N domains occurred in h -(BN)_{1-x}(C₂)_x epilayers with $x < 0.95$.

Raman spectroscopy measurements were also employed to study the phase separation effect as well as the bandgap opening in C-rich h -(BN)_{1-x}(C₂)_x alloys. Raman spectroscopy has been utilized previously as a non-destructive technique to study the phase separation and phase inhomogeneity in InGaN alloys.³⁰⁻³² Raman spectra of pure h -BN, graphite, and selected h -(BN)C samples are shown in Fig. 4(a). The graphite spectrum exhibits the typical characteristic graphitic E_{2g}(G) vibration peak at 1588 cm⁻¹ and the defect induced D peak at 1345 cm⁻¹.³³ The spectra of h -(BN)_{1-x}(C₂)_x epilayers with $x < 0.95$ (grown under the NH₃ flow rates of 1.4, 1.8, 2.2, 2.6, and 3.0 sccm) show that the G peak and the D peak are at the same positions as those in graphite. This suggests that separate C-C and B-N domains form and compositions in these h -(BN)C epilayers are phase separated and the C-rich material behaves similar to graphite. Moreover, the intensity and peak line width of the E_{2g} mode of these

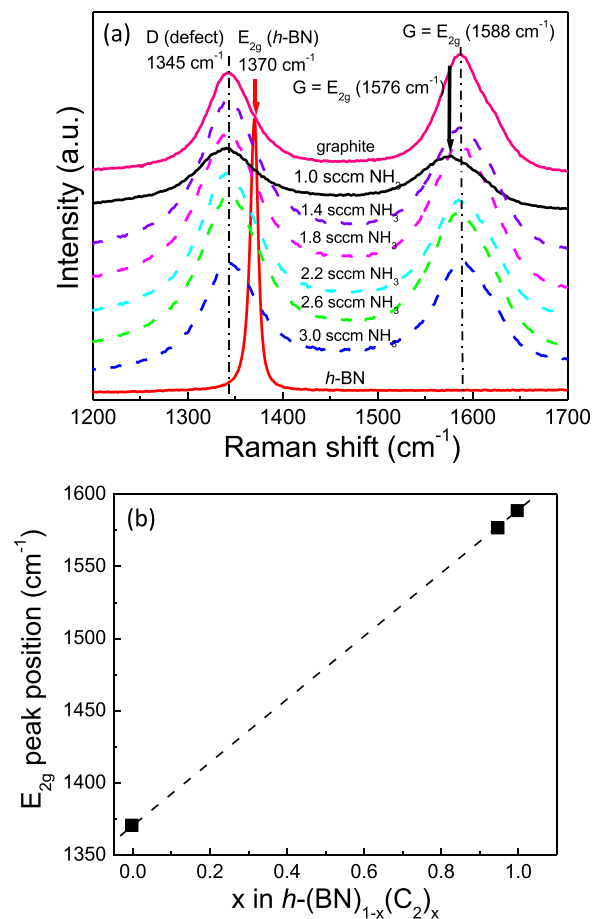


FIG. 4. (a) Raman spectra of h -BN ($x=0$), graphite ($x=1$), and selected h -(BN)_{1-x}(C₂)_x epilayers grown at different NH₃ flow rates. The G peak at 1576 cm⁻¹ of the h -(BN)_{1-x}(C₂)_x alloy with $x=0.95$ (1 sccm NH₃ flow rate) shifts towards the sp² bonded h -BN vibrational peak (1370 cm⁻¹), which is a signature of formation of homogenous h -(BN)C alloy. (b) E_{2g} vibration peak position vs. x in h -(BN)_{1-x}(C₂)_x showing peak positions for h -BN, graphite, and h -(BN)_{1-x}(C₂)_x alloy with $x=0.95$. The dashed line is a guide to the eyes.

samples are also similar to that of graphite. This is consistent with our conclusions obtained from the electrical transport measurement results presented in Fig. 3(b). In contrast, the Raman spectrum of $h\text{-(BN)}_{1-x}\text{(C}_2\text{)}_x$ alloy with $x=0.95$ (grown under 1.0 sccm NH_3 , black solid line) shows that the G peak shifted to 1576 cm^{-1} towards the characteristic of pure $h\text{-BN}$ peak (1370 cm^{-1}). Figure 4(b) plots the measured E_{2g} peak position vs. x in $h\text{-(BN)}_{1-x}\text{(C}_2\text{)}_x$ alloys. Typically the formation of homogeneous alloys causes a shift in the Raman spectral peak that varies linearly according to the peak positions of the constituent atoms or binary compounds.³² For homogeneous C-rich $h\text{-(BN)}_{1-x}\text{(C}_2\text{)}_x$ alloys, the Raman peak position is expected to shift towards lower frequency with a decrease of x . The observed Raman peak shift for $h\text{-(BN)}_{1-x}\text{(C}_2\text{)}_x$ alloy with $x=0.95$ thus corroborates the Hall-effect measurement results and further suggests the formation of homogeneous C-rich $h\text{-(BN)}_{1-x}\text{(C}_2\text{)}_x$ alloys with $x \geq 0.95$.

Phase separation is a very crucial issue towards the development of $h\text{-(BN)}_{1-x}\text{(C}_2\text{)}_x$ alloys.^{9,12} This is due to the bond energy difference among different atomic bonds in $h\text{-(BN)}_{1-x}\text{(C}_2\text{)}_x$ alloy: B-N (4.00 eV) > C-C (3.71 eV) > C-N (2.83 eV) > C-B (2.59 eV) > B-B (2.32 eV) > N-N (2.11 eV). Combining the present results with those of (BN)-rich $h\text{-(BN)}_{1-x}\text{(C}_2\text{)}_x$ alloys,⁹ we can conclude that $h\text{-(BN)}_{1-x}\text{(C}_2\text{)}_x$ epilayers with $0.032 < x < 0.95$ are most likely phase separated at a growth temperature of 1300°C . The phase diagram of the monolayer (BN)_{1-x}(C₂)_x alloys in the temperature range of 1500–3500 K suggests that the miscibility gap decreases with an increase in the growth temperature.¹² The same trend is expected for $h\text{-(BN)}_{1-x}\text{(C}_2\text{)}_x$ alloys. Combining our experimental results with that of calculation,¹² we have re-constructed in Fig. 5 the phase diagram for $h\text{-(BN)}_{1-x}\text{(C}_2\text{)}_x$ alloys, which can serve as a guideline for the further development of homogenous $h\text{-(BN)}_{1-x}\text{(C}_2\text{)}_x$ alloys. Due to the excellent matches in lattice constants and thermal expansion coefficients as well as high melting points throughout the entire alloys, it is expected that the alloy miscibility gap and degree of phase separation in $h\text{-(BN)}_{1-x}\text{(C}_2\text{)}_x$ alloys can be reduced or completely removed

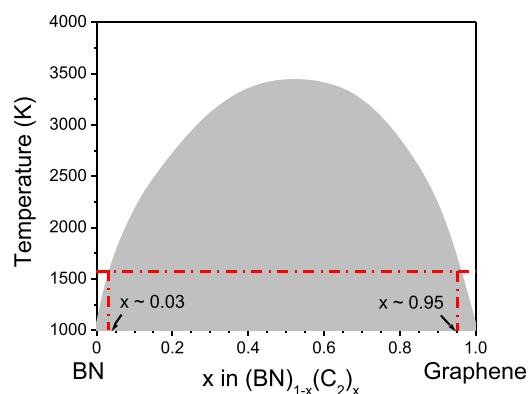


FIG. 5. Reconstructed phase diagram of $h\text{-(BN)}_{1-x}\text{(C}_2\text{)}_x$ alloys in the composition range ($0 \leq x \leq 1$) based on experimental results obtained for C-rich $h\text{-(BN)}_{1-x}\text{(C}_2\text{)}_x$ alloys in the present work, (BN)-rich $h\text{-(BN)}_{1-x}\text{(C}_2\text{)}_x$ alloys⁹ and calculation. Reproduced with permission from K. Yuge, Phys. Rev. B **79**, 144109 (2009). Copyright 2009 American Physical Society.¹² Experimental data for $h\text{-(BN)}_{1-x}\text{(C}_2\text{)}_x$ are indicated.

by increasing the growth temperature. Consequently, the overall material quality of $h\text{-(BN)C}$ alloys is expected to be improved by employing higher growth temperatures.

IV. CONCLUSIONS

In summary, we have synthesized C-rich $h\text{-(BN)}_{1-x}\text{(C}_2\text{)}_x$ epilayers using MOCVD and demonstrated that both p- and n-type conductivities can be obtained by changing the *stoichiometry* ratio between B and N through the variation of V/III ratio (or the NH_3 flow rate) employed during growth. We have observed intrinsic carrier conduction in $h\text{-(BN)}_{1-x}\text{(C}_2\text{)}_x$ samples with $x=0.95$, from which a bandgap energy of $E_g \sim 93\text{ meV}$ was deduced, which agrees almost perfectly with the expected value derived from the alloy dependence of the bandgap of $h\text{-(BN)}_{1-x}\text{(C}_2\text{)}_x$. The results suggest a bandgap opening in graphite through homogenous alloying with BN. Homogenous alloy formation has also been further confirmed from Raman spectroscopy measurements. Our experimental results revealed evidences that the critical BN concentration, x_{BN} , to open a small bandgap in graphite or to form $h\text{-(BN)C}$ homogenous alloy in the C-rich side is $\sim 5.0\%$ at a growth temperature of 1300°C . Since material synthesis and basic understanding of $h\text{-(BN)}_{1-x}\text{(C}_2\text{)}_x$ alloys are in the very early development stage, many issues merit further studies. For instance, based on the phase diagram shown in Fig. 5, further improvements in material quality would require higher growth temperatures above 1300°C to enable the synthesis of $h\text{-(BN)}_{1-x}\text{(C}_2\text{)}_x$ with broader alloy range without phase separation. Structural characterization techniques such as cross sectional transmission electron microscopy (TEM) would be very useful in addition to XRD to examine the crystalline quality of these layer structured films. However, the successful synthesis of homogeneous (BN)-rich and C-rich $h\text{-(BN)}_{1-x}\text{(C}_2\text{)}_x$ alloys ($3.2\% \geq x \geq 95\%$) by MOCVD at 1300°C already opens up possibilities to explore useful device applications in the deep UV and IR spectral regions.

ACKNOWLEDGMENTS

This work was supported by NSF (DMR-1206652). Jiang and Lin are grateful to the AT&T Foundation for the support of Ed Whitacre and Linda Whitacre endowed chairs. The authors are grateful to Dr. Kate Ziemer for valuable discussions on XPS results.

¹N. G. Chopra, R. J. Luyken, K. Cherrey, V. H. Crespi, M. L. Cohen, S. G. Louie, and A. Zettl, *Science* **269**, 966 (1995).

²A. Rubio, J. L. Corkill, and M. L. Cohen, *Phys. Rev. B* **49**, 5081 (1994).

³K. Watanabe and T. Taniguchi, *Phys. Rev. B* **79**, 193104 (2009).

⁴K. Watanabe, T. Taniguchi, and H. Kanda, *Nat. Mater.* **3**, 404 (2004).

⁵R. Dahal, J. Li, S. Majety, B. N. Pantha, X. K. Cao, J. Y. Lin, and H. X. Jiang, *Appl. Phys. Lett.* **98**, 211110 (2011).

⁶S. L. Rumyantsev, M. E. Levinshtein, A. D. Jackson, S. N. Mohammad, G. L. Harris, M. G. Spencer, and M. S. Shur, in *Properties of Advanced Semiconductor Materials GaN, InN, BN, SiC, SiGe*, edited by M. E. Levinshtein, S. L. Rumyantsev, and M. S. Shur (John Wiley & Sons, Inc., New York, 2001), pp. 67–92.

⁷V. L. Solozhenko, *Properties of Group III Nitrides*, EMIS Data-reviews Series, N11, edited by J. H. Edgar (INSPEC, 1994), pp. 43–70, and references therein.

⁸A. I. Savvatimskiy, *Carbon* **43**, 1115 (2005) and references therein.

⁹M. R. Uddin, S. Majety, J. Li, J. Y. Lin, and H. X. Jiang, *J. Appl. Phys.* **115**, 093509 (2014).

- ¹⁰S. Bahandary and B. Sanyal, *Graphene-Boron Nitride Composite: A Material with Advanced Functionalities* (InTech, 2012).
- ¹¹H. Nozaki and S. Itoh, *J. Phys. Chem. Solids* **57**, 41 (1996).
- ¹²K. Yuge, *Phys. Rev. B* **79**, 144109 (2009).
- ¹³M. R. Uddin, T. C. Doan, K. S. Ziemer, J. Li, J. Y. Lin, and H. X. Jiang, *AIP Adv.* **4**, 087141 (2014).
- ¹⁴L. Ci, L. Song, C. Jin, D. Jariwala, D. Wu, Y. Li, A. Srivastava, Z. Wang, K. Storr, L. Balicas, F. Liu, and P. M. Ajayan, *Nat. Mater.* **9**, 430 (2010).
- ¹⁵A. C. Gomez, M. Wojtaszek, A. Arramel, N. Tombross, and B. J. Wees, *Small* **8**, 1607 (2012).
- ¹⁶M. S. Dresselhaus and G. Dresselhaus, *Adv. Phys.* **51**, 1 (2002).
- ¹⁷O. Bierwagen, T. Ive, C. G. Van de Walle, and J. S. Speck, *Appl. Phys. Lett.* **93**, 242108 (2008).
- ¹⁸A. Kumar, J. Pernot, F. Omnès, P. Muret, A. Traoré, L. Magaud, A. Deneuve, N. Habka, J. Barjon, F. Jomard, M. A. Pinault, J. Chevallier, C. Mer-Calfati, J. C. Arnault, and P. Bergonzo, *J. Appl. Phys.* **110**, 033718 (2011).
- ¹⁹S. Majety, T. C. Doan, J. Li, J. Y. Lin, and H. X. Jiang, *AIP Adv.* **3**, 122116 (2013).
- ²⁰G. W. Semenoff, *Phys. Rev. Lett.* **53**, 2449 (1984).
- ²¹X. K. Cao, B. Clubine, J. H. Edgar, J. Y. Lin, and H. X. Jiang, *Appl. Phys. Lett.* **103**, 191106 (2013).
- ²²G. M. Metzger, R. A. Stall, C. E. C. Wood, and L. F. Eastman, *Appl. Phys. Lett.* **37**, 165 (1980).
- ²³T. J. de Lyon, J. M. Woodall, M. S. Goorsky, and P. D. Kirchner, *Appl. Phys. Lett.* **56**, 1040 (1990).
- ²⁴D. Wei, Y. Liu, Y. Wang, H. Zhang, L. Huang, and G. Yu, *Nano Lett.* **9**, 1752 (2009).
- ²⁵Y. B. Tang, L. C. Ying, Y. Yang, X. H. Bo, Y. L. Cao, H. E. Wang, W. J. Zhang, I. Belo, S. T. Lee, H. M. Cheng, and C. S. Lee, *ACS Nano* **6**(3), 1970 (2012).
- ²⁶M. Razeghi, *Fundamentals of Solid State Engineering* (Springer Science+Business Media LLC, 2009), Chap. 7.
- ²⁷H. Gao, L. Song, W. Guo, L. Huang, D. Yang, F. Wang, Y. Zuo, X. Fan, Z. Liu, W. Gao, R. Vajtai, K. Hackenberg, and P. M. Ajayan, *Carbon* **50**, 4476 (2012).
- ²⁸P. P. Shinde and V. Kumar, *Phys. Rev. B* **84**, 125401 (2011).
- ²⁹M. O. Watanabe, S. Itoh, T. Sasaki, and K. Mizushima, *Phys. Rev. Lett.* **77**, 187 (1996).
- ³⁰S. Hernandez, R. Cusco, D. Pastor, L. Artus, K. P. O'Donnell, R. W. Martin, I. M. Watson, Y. Nanishi, and E. Calleja, *J. Appl. Phys.* **98**, 013511 (2005).
- ³¹A. Kar, D. Alexson, M. Dutta, and M. A. Stroscio, *J. Appl. Phys.* **104**, 073502 (2008).
- ³²S. R. Meher, K. P. Biju, and M. K. Jain, *Phys. Status Solidi A* **208**, 2655 (2011).
- ³³S. Reich and C. Thomsen, *Phil. Trans. R. Soc. London A* **362**, 2271 (2004).